Review of Scientific Instruments (2008), in print.

A photoelectron–photoion coincidence imaging apparatus for femtosecond time-resolved molecular dynamics with electron TOF resolution of σ=18 ps and energy resolution ΔE/E=3.5%

Arno Vredenborg, Wim G. Roeterdink, and Maurice H.M. Janssen*

Laser Centre and Department of Chemistry,

Vrije Universiteit, de Boelelaan 1083,

1081 HV Amsterdam, The Netherlands

(Dated: May 29, 2008)

Abstract

We report on the construction and performance of a novel photoelectron-photoion coincidence machine in our laboratory in Amsterdam to measure the full three-dimensional momentum distribution of correlated electrons and ions in femtosecond time-resolved molecular beam experiments. We implemented sets of open electron and ion lenses to time stretch and velocity map the charged particles. Time switched voltages are operated on the particle lenses to enable optimal electric field strengths for velocity map focusing conditions of electrons and ions separately. The position and time sensitive detectors employ micro-channel-plates (MCP) in front of delay line detectors. A special effort was made to obtain the time-of-flight (TOF) of the electrons at high temporal resolution using small pore (5μm) MCPs and implementing fast timing electronics.

We measured the TOF distribution of the electrons under our typical coincidence field strengths with a temporal resolution down to σ=18 ps. We observed that our electron coincidence detector has a timing resolution better than σ=16 ps, which is mainly determined by the residual transit-time-spread of the MCPs. The typical electron energy resolution appears to be nearly laser bandwidth limited with a relative resolution of $\Delta \mathrm{E}_{FWHM}/\mathrm{E} = 3.5\%$ for electrons with kinetic energy near 2 eV. The mass resolution of the ion detector for ions measured in coincidence with electrons is about $\Delta \mathrm{m}_{FWHM}/\mathrm{m} = 1/4150$. The velocity map focusing of our extended source volume of particles, due to the overlap of the molecular beam with the laser beams, results in a parent ion spot on our detector focused down to $\sigma = 115$ μm.

*Corresponding author. E-mail: mhmj@chem.vu.nl

I. INTRODUCTION

The first application of spatially sensitive single particle detectors in molecular photodissociation by Chandler and Houston two decades ago[1] was the beginning of an new era in molecular dynamics and spectroscopy.[2] During the last decade there has been a strong interest to measure the full three-dimensional momentum distribution of coincident ions and electrons ejected in a molecular dynamical process.[3–14] The detectors employed in these experiments are usually based on position and time sensitive single particle detectors consisting of micro-channel-plates (MCP) and delay line or cross-strip anodes.[15–17]

Recently, there have been various efforts to improve the spatial resolution of the measured distributions of electrons and ions ejected from an extended source region of the particles using additional focusing lenses. In many cases some form of velocity map imaging[18] of the charged particle trajectories is used to focus trajectories with the same momentum originating from a source region several mm length onto a much smaller spot on the detector.

Besides the efforts to improve the spatial resolution there have been developments to improve the temporal resolution of the MCPs and electronics used to measure the time-of-flight (TOF) of the particle at the detector. In some cases the TOF is measured from the transient signals of the delay lines using time-to-digital-converters (TDC). In those cases fast multi-channel TDC electronics are needed to measure all the spatially encoding delay line signals with high temporal resolution. Recent developments in highly accurate timing clocks[19] have been implemented in multi-channel (8 or 16 channels typically) timing boards with a resolution down to 20 ps.[20] Even though these timing boards have in principle a very high resolution timing bin, the measured resolution of the TOF from the average of the time-sum of delay line signals has usually been specified to be no better than about 100 ps.[21] A second technique to measure the TOF of the particles is to use an additional pickup signal from the MCP when the particle hits the detector. This pickup signal is amplified and usually processed by a constant-fraction-discriminator (CFD) and a high resolution time-to-amplitude (TAC) device. State-of-the-art integrated CFD/TAC boards were reported to have electronic resolutions down to $\sigma = 4.1$ ps.[22] The ultimate single particle temporal detection resolution is determined by the transit-time-spread of micro-channel-plate detectors[23], the quality (i.e. low walk) of the CFD used to process the pickup signal and the accuracy and resolution of the TAC.[24]

In this paper we report on the design and performance of a newly constructed photoelectron-photoion coincidence detector for femtosecond time-resolved coincidence experiments on molecules. The apparatus employs a doubly skimmed molecular beam which is crossed by tunable multi-color femtosecond laser pulses and two position and time sensitive detectors on opposite sides of a specially designed lens. We use pulsed electric fields for optimum spatial and temporal resolution of electron and ion trajectories. We especially focussed to achieve a high temporal resolution of the TOF of the detected electrons and combined improvements in implementation of ion focusing optics, temporal response of small pore micro-channel-plates and state-of-the-art TAC and TDC electronics. The result of these efforts is a timing resolution for the observed coincident single electron hits from our extended source region down to σ=18 ps on a typical electron TOF of 15 ns. The high resolution detection of the three-dimensional momentum coordinates of the electrons enables the measurement of high resolution electron images in coincidence with high resolution ion images.

The paper is structured as follows. In Section II we give a description of the design of the new molecular beam apparatus and the implementation of the detection equipment synchronized to our femtosecond laser system running at a repetition rate of 5 kHz. In Section III we give a detailed report on the spatial and mass resolution of the ion images, and the spatial and temporal specifications of our coincident electron detector. Furthermore, we illustrate the performance of the new photoelectron-photoion coincidence apparatus with representative images for femtosecond photodynamics in Xe, NO and NO_2.

II. APPARATUS

A. The vacuum apparatus and molecular beam

The UHV vacuum machine consists of three differentially pumped chambers, a source, buffer and imaging chamber, see Fig. 1. To reduce as much as possible any contamination of the vacuum system we use oil free pumps in the whole vacuum apparatus. After the machine has been vented and opened for modifications we typically bake the whole apparatus to about 120^0C to reach optimum vacuum. The three chambers are pumped by magnetically levitated turbo molecular pumps, the source chamber has a 1250 l/s turbo drag pump (Alcatel ATH

1300 MT), the buffer chamber a 400 l/s (ATH 400 MT) and the imaging chamber a 2100 l/s (ATH 2300 MT) pump. All turbo pumps are backed by a single five stage oil free roots pump (Alcatel ACP28G). A removable liquid nitrogen trap between the turbo pumps and the roots pump prevents corrosive gasses from entering the forepump. The last four stages of the forepump are continuously purged with nitrogen gas. With the molecular beam off the base pressures are 5.10^{-9} mbar in the source chamber, 1.10^{-9} mbar in the buffer chamber and $<5.10^{-10}$ mbar in the detection chamber.

A nozzle with a diameter of 100 μm is located in the source chamber to produce a continuous molecular beam. The typical backing pressure behind the nozzle is 1.0 bar. The molecular beam is doubly skimmed (BeamDynamics) with the first skimmer (diameter 1 mm) positioned about 2 cm downstream of the nozzle. The second skimmer (diameter 200 μm), which separates the buffer chamber from the imaging chamber, is located about 12 cm downstream of the first skimmer. With the molecular beam on the pressure in the imaging chamber increases to about 2-4$\times 10^{-9}$ mbar. The molecular beam is crossed about 45 cm downstream of the nozzle by the femtosecond laser pulses. A lens (typically with focal length of 30-50 cm) focusses the laser waist down to about 100-150 micron in diameter. From the geometry and location of our skimmers we estimate that the laser crosses the molecular beam in the direction of the laser propagation along a length of about 1 mm. Light baffles are mounted at the entrance and exit ports of the laser beams to reduce scattered UV laser light from reaching the detectors. The incoming laser beam is doubly skimmed using home built conical skimmers with a diameter of 2 mm.

B. Photoelectron-photoion coincidence detector

After interaction of the molecules with the femtosecond laser pulses, the electrons and ions are extracted by lenses into two opposite TOF tubes. In Fig. 2 we give a schematic drawing of the geometry of our lenses and the TOF tubes. The electron TOF tube and the lenses are shielded from the earth magnetic field by a 1 mm thick μ-metal tube.

All electrodes are open and the TOF tubes and the front MCP plate of both detectors are at ground potential. Besides the standard repeller and extractor lenses for velocity map imaging we added for both the electrons and the ions an extra lens, L_e and L_i, respectively, to enable lower extraction voltages in the region where the electrons and ions are formed.

Furthermore, these lenses make it possible to compensate for the somewhat distorted field for velocity map imaging due to the relatively large open diameter on the repeller lenses. In principle, when setting the voltages for optimal electron velocity mapping the ion lens L_i can be operated at higher negative voltage to make the field at the open position of the electron repeller R_e (is also ion extractor plate E_i, see Fig. 2) more homogeneous. For the results presented in this paper we did not implement this extra feature yet, and switched the ion lens L_i from zero voltage when we detect the electrons.

In order to have optimal voltages and extraction field strength for both electrons and ions we operate the lenses in a pulsed mode at the 5 kHz repetition rate of our experiment. Because the typical electron TOF is about 15 ns and the ion TOF is of the order of several μs for each laser shot we initially set the lenses R_e, E_e and L_e for the voltages to image the electrons. Typically, R_e=-520 V, E_e=-385V, L_e=-270 V and the voltages are carefully adjusted for optimum electron images. These lens voltages enables the detection of electrons with kinetic energies up to 3-3.5 eV perpendicular to the TOF axis. Subsequently, about 50 ns after detection of the electron, the polarity of the lenses R_e=E_i and E_e=R_i are switched to velocity map the coincident ion on the second detector. The HV-switches consist of Behlke switches (HTS-51) and within 100 ns the polarity is completely reversed to maintain optimum voltages for the ion trajectories. The lenses remain at positive voltages for about 15 microseconds and subsequently the polarity is switched back again within 100-150 μs to the initial settings for optimum electron imaging. The ions are most efficiently detected by MCPs with significant impact energy (>1000 eV).[25] Therefore, the ions are accelerated typically with R_i=2000 V, E_i=1550 V and L_i=750 V on the ion lens. These acceleration voltages in combination with our ion TOF length allows the measurement of fragments with a kinetic energy up to 2 eV. For higher kinetic energies the acceleration voltages can be increased.

At the end of the TOF tubes two position- and time-sensitive particle delay line detectors (Roentdek[21] large anode DLD40X) are mounted with the TOF axis perpendicular to the molecular beam. Both detectors have 40 mm active diameter MCPs mounted in a Chevron configuration. The front of the input MCP of both detectors is grounded to prevent stray electric fields from penetrating the field free TOF region. The MCPs for the electron detector, Det_e, have 5μm pore channels (L:D=60:1) biased at 12 degrees and the front plate has an additional MgO coating for optimum electron detection. The extra benefit of the

MgO coating is the reduced sensitivity of the MCP for scattered UV radiation from the laser pulses. The MCPs of the ion detector, Det_i, have 12.5μm pore channels (L:D=80:1). To compensate for the translation of the ion sphere because of the center-of-mass movement of the ions in the direction of the molecular beam velocity we moved the ion detector Det_i about 7-8 mm relative to the electron detector Det_e.

The delay line signals are processed by a differential input 8 channel front-end CFD (ATR19-8-NIM) and the 8 NIM output signals are fed into a high-resolution TDC board using the CERN HPTDC[19] chip (TDC8HP). The least-significant-bit (LSB) of this TDC is specified as 25.0 ps and the TDC has a double hit dead-time of less than 10 ns.[21] The common trigger of the TDC channels is produced by a photodiode with an integrated CFD producing a NIM output pulse (Becker&Hickl OCF-401). A homebuilt fast OR-gate processes the optical trigger and one of the ion delay line signals into a single channel of the 8-channel TDC. The position information in x or y direction is obtained for each detector by using the time difference of the two x or y TDC delay line signals and a conversion of 1.9 ns / mm.[21]

To obtain a better accuracy of the electron TOF signal than can be obtained from the time sum of the TDC signals, we use a pickup signal from the back MCP plate of the electron detector. This signal is AC-coupled by a capacitor into a 50 Ohm cable to a SMA vacuum feedthrough. The pickup signal has a typical amplitude of about 15 mV in 50 Ohm. The signal is pre-amplified and processed by an integrated CFD/TAC (Becker&Hickl SPC-130). We operate the TAC in reverse start-stop mode, i.e. the electron pickup signal starts the TAC and a delayed trigger from a fast photodiode is used as the stop signal. Because the travel time of the pickup signal may be dependent on the exact position of the impact on the MCP relative to the position of the pickup lead, we correct for each electron event the measured TAC TOF value for the distance between the impact on the MCP (known from the delay line position coordinates) and the pickup lead from the back plate. The maximum difference in the distance between two events with our diameter MCPs is 40 mm. If we assume that the travel time of this transient MCP back potential to the pickup lead on the MCP is determined by the linear distance between these two points a distance of 40 mm corresponds to a difference in travel time for the voltage pickup pulse of 40 mm / propagation speed. In our data analysis we find an optimum correction of our electron TOF from the asymmetry in the arrival time distribution using a pickup propagation speed of 0.7 times the speed of light. It means for a maximum position difference of 40 mm it can amount to

a TOF correction of 190 ps maximum.

The signals from the TDC and TAC boards are synchronized using time stamps in our home written data acquisition programme. A valid photoelectron-photoion coincident event is received when all 8 channels of the TDC and the single TAC channel have an event recorded. The typical coincidence rate in our experiments is about 0.02-0.05 per laser shot, which means we have a typical number of coincidence events of 100-250 events/s at the 5 kHz repetition rate of our femtosecond laser system.

C. The femtosecond laser system

The femtosecond laser system (Spectra Physics) consists of a Titanium-Sapphire oscillator (Mai-Tai) which seeds the chirped regenerative amplifier (Spitfire Pro). The regen amplifies the seed oscillator pulses to 500 μJ at a repetition rate of 5 kHz. A small percentage of the regen is split off and monitored online with a homebuilt single shot SHG autocorrelator equipped with a CCD camera. The shortest pulse obtainable from the regen system is about 130 fs. The color of the frequency doubled and frequency tripled pulses is monitored with a spectrum analyzer (Ocean Optics). Typical pulse energies used are 4 μJ for the probe laser (266 nm) and 15 μJ for the pump laser (400 nm). A CCD camera is used to estimate the size of the focus of about 90 μm of both pump and probe laser. The 800 nm regen pulses can also be used to pump two independent homebuilt noncollinear-opto-parametric-amplifiers (NOPA) to generate short (25-30 fs) tunable laser pulses in the visible wavelength region. To demonstrate the performance of the coincidence detector we will present in this paper only data using the second (400 nm) and third (266 nm) harmonic of the 800 nm regen laser.

III. RESULTS AND DISCUSSION

A. Spatial and mass resolution of coincident ions

The pitch of the wires of the DLD40X delay line is 1 mm. With the minimal digitizing resolution of the TDC of 25 ps and the time to position conversion of 1.90 ns/mm[21] the theoretical spatial resolution of the detectors is about $25/1.9 = 13$ μm, close to the 12.5 μm pore diameter of the ion MCPs. This assumes that the quality of the delay line signal, that is formed by the overlapping contributions of multiple wires spaced at the 1 mm pitch from the

extended electron footprint from the exit of the MCP, and the quality of the ATR-19 CFD is so good as to not contribute to additional broadening of the spatial resolution. It has been shown before that cross-strip anodes with a pitch of 500 μm can reach a spatial resolution of about 1/100 of the pitch diameter and were limited by the ultimate pore diameter of the entrance MCP of about 7 μm.[26]

However, in our application the spatial resolution is limited by the quality of the velocity map imaging of the ion trajectories due to the extended source of the ions and electrons. In Fig. 3 we show the Time-Of-Flight spectrum of the Xenon isotopes as determined from the time-sum of the delay line signals of the ion detector. The ions were produced by a four photon absorption of a 400 nm femtosecond laser pulse and were measured in coincidence with electrons by switching the voltages on the ion lenses as discussed in Section II B. The individual isotope peaks have a FHWM of 2 ns giving a mass resolution at the Xe mass of Δm/m = 1/4150. This mass resolution can be up to a factor of two better, Δm/m $\approx$ 1/8000, in static conditions. This is due to some additional spreading introduced by the changing voltages on the ion lenses when the voltages are switched to the ion geometry after the arrival of the coincident electron.

The lack of internal degrees of freedom in Xenon ensures that all the excess energy is converted into kinetic energy of the electron. The ion image of Xenon reflects the focusing resolution of the ion optics and is shown in Fig. 4. The spatial size of the parent ion in x and y-directions are indicated in the graphs next to the x-y image. The image size in the direction of the laser propagation direction, y-direction, can be fitted to a Gaussian with σ = 115 μm (FWHM = 270 μm).[27] This represents the best focussing conditions of our velocity map apparatus in coincident imaging mode. This means that we focus the initial spot of about 1 mm length, due to the crossing of the laser beam with the molecular beam, to a spot size about 5 times smaller on the ion detector.

The best possible resolution for both the time and position detection of the charged particles is achieved with a point source of particles. However, experimentally the source is determined by the interaction region of the molecular beam with the laser, which crosses the molecular beam at 90 degrees. In our case, the laser beams are typically focussed to about 90 μm (FWHM of the focus of the intensity distribution fitted to a Gaussian shape) or somewhat less. The calculated Rayleigh length is about 7 cm for a Gaussian laser beam with 90 μm waist at a wavelength of 400 nm. In case of multiphoton transitions the effective

length of the laser focus will be shorter, but under all our experimental conditions the effective source region along the laser propagation direction is bounded by the diameter of the molecular beam at the laser crossing which is about 1 mm. This crossing of the focussed laser beam with the molecular beam at 90 degrees results in a cylindrically shaped source region. It defines an upper bound to the size of the source along the time-of-flight axis and in the direction of the molecular beam of about 90 μm. This effective source region of ions may even be smaller than 90 μm for multiphoton excitations. Along the propagation direction of the laser beam the source region has a length of about 1 mm, i.e about ten times larger. Decreasing the size of the molecular beam improves the spatial resolution as well as the time resolution, but also decreases the number of molecules due to a smaller source volume of particles.

Velocity map imaging partially solves the problem of the relatively large spatial extension of the source region along the laser propagation direction. From SIMION simulations of our ion lenses we find that the TOF-difference of two Xe-ion trajectories starting in the source region $\pm$50 μm displaced along the TOF axis on either side of the centre point of our source region is about 2 ns for Xe^+ ions with a forward molecular beam velocity of 0.213 eV (Xe seeded in Ar going at 560 m/s). The time difference is equal to the experimentally obtained value and is not compromised much under the velocity map imaging conditions. For extensions up to about $\pm$500 μm on either side of the centre along the propagation direction of the laser it increases to about 2.5 ns according to SIMION simulations. Therefore, no special Wiley-McLaren conditions[28] have to be applied to achieve a better time resolution as was done by Lebech *et al.*[8] However, for larger interaction regions in both directions the velocity mapping condition starts to reduce the time resolution more strongly. Therefore, it is recommended to limit the length of the velocity map region to 1 mm or less by properly skimming the molecular beam. In our set-up we have positioned a rather small second skimmer of 200 μm diameter (see Section II A).

The velocity distribution along the direction of the molecular beam is limiting the spatial resolution in the x-direction. The molecules of study are typically seeded in Argon and are traveling at a final speed of about 560 m/s. As can be seen in Fig. 4 a Gaussian fit to the spatial distribution along the molecular beam direction gives a spatial resolution of σ = 285 μm (FWHM = 670 μm). From the displacement on the ion detector of the position of the focussed parent ion spot (ions from ionization of moving Xe atoms in the

seeded beam) relative to the position of the ion spot from ionization of thermal background gas, we can calculate the conversion from distance to ion velocity. The width of the ion focus in the direction of the molecular beam represents a FWHM velocity spread of about 85 m/s. This is a very typical velocity spread for a continuous molecular beam expansion with 1 bar behind a 100 μm nozzle. In principle, this extension along the molecular beam can be reduced by using beams with better longitudinal translational cooling. This can be achieved for instance with higher backing pressures and we are currently working to develop a pulsed molecular valve for operation at 5 kHz to obtain higher beam intensities and lower translational velocity spread along the molecular beam direction. However, for experiments employing femtosecond velocity map ion imaging[29–31] it appears that the fragment ion kinetic energy distribution in femtosecond time-resolved experiments of polyatomic molecules is rather broad without sharp features due to the many internal degrees of freedom in the polyatomic fragment where the residual of the energy can be deposited. This means that the presently obtained velocity resolution for the ionic fragment is sufficient.

B. Electron single hit TOF resolution

Recently, there have been reports on the implementation[17,32] and design performance goals[33] of a high resolution TOF and momentum detector for photons and electrons. The realized TOF resolution of this cross-strip anode for the detection of scattered photons from a synchrotron source was reported to be $\sigma = 55$ ps (FWHM = 130 ps).[32] In the high-energy physics community there is presently an effort to develop fast MCP based multi-anode photon detectors for Cherenkov radiation from high energy particles with the ultimate goal of a time-of-flight resolution of a multi-photon event near $\sigma = 1$ ps.[34] At present the best reported result for detection of the TOF of multiple photons from a single high energy 3GeV pion-beam particle is about σ=6 ps.[22]

In the development of our new photoelectron-photoion coincidence imaging apparatus we put a strong effort to obtain a high-resolution for the TOF of the coincident single electron as measured with our MCP delay line electron detector. The typical acceleration voltages that are employed to measure the three-dimensional momentum distribution of photoelectrons with energies up to 2 eV are R_e=-520 V, E_e=-385V, L_e=-270 V. If electrons with 3-3.5 eV are ejected in a direction perpendicular to the TOF axis they will still fall within the 40 mm

diameter of our MCP using these lens voltages. We measured the electron TOF resolution under these normal acceleration conditions. In Fig. 5 we show the arrival time distribution of electrons in coincidence with Xe^+ ions as obtained (for the same events) by the pickup signal and the TAC (panel a) versus the delay line signal and the TDC (panel b). The electrons are produced by 4-photon ionization of Xe by a 130 fs laser pulse at 400 nm. The polarization of the laser was oriented along the TOF direction. This results in the production of forward (in the direction of the electron detector) ejected electrons and backward (in the direction of the ion detector) ejected electrons. So for each coincident (e,Xe^+) event we have for the electron TOF 4 delay line timing signals obtained by the TDC (2 for the x-position and 2 for the y-position) and 1 pickup signal processed by the TAC.

The time difference between the forward and backward ejected electrons is mainly determined by the extraction field strength, $E_{extract}$. A lower extraction field leads to a larger difference in arrival time between particles of mass m ejected in the forward (towards detector) or backward (away from detector) direction, T_{FB}. This time difference T_{FB}, due to an initial kinetic energy E_{kin} of the charged particle of mass m, can be estimated with the help of a simple formula $T_{FB} \approx \sqrt{8 * m * E_{kin}}/qE_{extract}$. This means that the lower the extraction field the larger the forward-backward time difference T_{FB}. This is the reason we added an extra lens, L_e, to the standard velocity map lenses, see Fig. 2. It enables us to do 'slow' field extraction of the electrons, and at the same time preserve velocity map imaging conditions. For instance, using the formula above (and also supported by more exact SIMION trajectory simulations), we find for a coincident (with Xe^+ ions) electron with kinetic energy of E_{kin} = 0.285 eV, formed in an extraction field of $E_{extract}$ = 6.7 V/mm, that the time difference is T_{FB} = 540 ps. This field of 6.7 V/mm is the field, according to SIMION simulations, in the laser interaction region of our lenses using the voltages of R_e=-520 V, E_e=-385V, L_e=-270 V on the lenses, see Fig. 2. Note that due to the rather open structure of our repeller and extractor electrodes the field in the centre between repeller and extractor is lower than the field calculated for a simple fully closed parallel plate capacitor spaced at a distance between repeller and extractor of 15 mm (≈135 V/15 mm = 9 V/mm). We observe experimentally a forward-backward time of T_{FB} = 540 ps (Fig. 5), exactly as calculated. We used our same physical electrodes also in standard velocity map mode, i.e. with only a repeller and an extractor and no extra lens electrode. For standard velocity map mode we observed experimentally velocity map imaging of the electrons for R_e=-520 V, E_e=-315 V, L_e=0 V,

and a forward-backward time difference of only $T_{FB} \approx 320$ ps. It means the slow extraction geometry, as implemented here using the extra lens L_e, in comparison to standard velocity map imaging with repeller and extractor plates only, enables us to reduce the extraction field substantially. The lower field stretches the forward-backward time difference from 320 ps to 540 ps, i.e. by almost 70% and still enables us to do velocity map imaging of electrons with similar maximum kinetic energy up to 3-3.5 eV. We have taken electron images (not shown here) with the three lenses, R_e, E_e and L_e, set at an even lower extraction field of 4.8 V/mm, which is close to the minimum field strength needed to still be able to velocity map electrons with $E_{kin} = 2.0$ eV on the detector with sufficient spatial resolution. This lower field results in a forward-backward time stretched to 750 ps for electrons with 0.285 eV. In summary, the extra electrode L_e, lengthens the forward-backward time while preserving velocity map imaging conditions and as such provides a better time resolution.

As can be seen in panel a) of Fig. 5 the arrival time distribution of the electrons as measured from the pick-up signal and the TAC can be fitted to a Gaussian shaped distribution with a resolution of $\sigma = 18$ ps for the backward ejected electrons and $\sigma = 20$ ps for the forward ejected electrons. The coincident electrons were selected to arrive within a spatial region of about 1.37 mm^2 (a radius of 50 TDC units = $50 \cdot 25$ / $1.9 = 660$ μm) centered around the TOF normal of the electron detector. The (x,y) position of the electron events were obtained from the delay line signals and the time difference of the TDC flight times.

In panel b) we show the TOF for the same selected electron events as obtained from the average of the two x-direction delay line TDC measurements. As can be seen by comparison the TAC measurement gives about a factor of 2.5 better timing resolution than the TDC. We believe that our electron TOF resolution of $\sigma = 18$ ps is the best TOF resolution reported so far for detection of electrons in a coincidence imaging set-up. For the slow electrons of 0.285 eV with a $T_{FB} = 540$ ps it represents a relative time resolution of $18/540 = 3.3\%$ along the TOF direction. For electrons with much higher kinetic energy up to about 3 eV the T_{FB} increases to $\approx \sqrt{10} \cdot 540 = 1700$ ps at our typical lens voltages. It means that for 3 eV electrons ejected along the TOF axis our coincidence detector has a relative time resolution of about 1%.

It is interesting to note that the forward electron peak has a slightly higher intensity. We are operating at an average count rate of about 250 counts/s so the average time between two electron hits is about 4 ms. If we assume that a single electron hit in the entrance

channel of the front MCP leads to the excitation of 7 channels of the back MCP plate of the electron detector, we estimate that each hit occupies an area with a radius of about 8.5 μm of the back MCP. As most of the intensity of the signal is for events near the center of the image this may lead to slightly less gain efficiency of the MCP for backward ejected electrons due to the gain recovery time of several (tens of) ms of a single MCP channel.[35]

To test our limiting TOF resolution we also measured the distribution for much higher acceleration voltages. These voltages are normally not needed in our experiments, but if one would have a molecular or atomic system that produces electrons with much higher kinetic energy such higher voltages can be applied. In Fig. 6 we show the relative TOF of the forward and backward ejected electrons produced in the same way as in Fig. 5 but accelerated in velocity map mode with a field strength of about 19 V/mm. As can be seen the forward-backward time is reduced to only 188 ps. And the resolution that is obtained is slightly improved to σ = 16 ps. We think that the single electron TOF resolution of 16 ps is presently mainly limited by the transit-time-spread (TTS) of the MCPs used in our electron detector and the residual TOF spread due to the extension of our source region of electrons.

We have performed SIMION simulations to estimate the contribution of the extended source region along the TOF axis. If we use a laser focus diameter of 100 μm and two forward ejected electrons with either (0.285 + 0.019) eV or (0.285 - 0.019) eV at two positions spaced Δl=100 μm apart the simulation calculates a difference in arrival time of 15 ps. If we take this time difference to represent the FWHM contribution due to the spatial extension along the TOF axis, we find the contribution to the resolution due to the spatial time difference of $\sigma_{\Delta l}$ = 15/2.355 = 7 ps. If we subtract the contributions from the electronics ($\sigma_{TAC} \approx 4.1$ ps[22]) and the Δl=100 μm source region we obtain σ_{TTS}(experimental) = $\sqrt{(16^2 - 4.1^2 - 7^2)}$ = 14 ps. The transit time in the MCP pores is equal to the sum of inter collision times in the micro channels.[36] The transit-time-spread (TTS) increases linearly with the length of the plates and is inversely related to the square root of the acceleration field over the MCP channel. Therefore, small pores and small Length-to-Diameter (L/D) ratio are prefered for a good TOF temporal resolution, i.e. a Chevron configuration is preferred over a Z-stack. We estimate the theoretical TTS of our 5 μm, L:D=60:1 Chevron MCP set by comparison with the scaling laws[23] and find σ_{TTS}(theoretical,Chevron,5μm, L:D=60:1)= 20 ps (FWHM = 46 ps). This is in reasonable agreement with the experimentally estimated σ_{TTS}(experimental)

= 14 ps, and it appears that the TTS largely accounts for the total resolution σ = 16 ps observed in the electron detection of our coincidence imaging spectrometer.

C. Electron energy resolution

In Fig. 7 we show two electron images obtained in two different experiments on Xe atoms (panel A) and NO molecules (panel B) with femtosecond pulses near 400 nm and 266 nm at time overlap. The electron images were measured using our typical acceleration voltages (see Fig. 5) with the polarization of both lasers along the detector plane. Various rings can be observed due to various multi-photon processes. Xe is often used to calibrate our electron images. The typical FWHM bandwith of our femtosecond pulses is about 19 meV at 400 nm and 26 meV at 266 nm. The electron peak at E=0.28 eV, labeled (a) in panel C, results from ionization of Xe by a 2 photon excitation with 266 nm photons plus a one photon excitation with 400 nm photons. The experimentally observed FWHM = 41 meV. This is exactly the width that would be expected for this multi-photon excitation process due to the finite width of our fs laser pulses, FWHM = $\sqrt{(19^2 + 26^2 + 26^2)}$ = 41 meV. It means the resolution at these low energies is purely laser bandwidth limited. For the electron peak at 1.87 eV, labeled (c) in panel C, which results from an ionization of Xe with 1 photon of 266 nm and 3 photons of 400 nm (or 3 photons of 266 nm and 0 photons of 400 nm, this is equal in energy) we observe an experimental resolution of FWHM = 65 meV. From the photon process we would expect FWHM = $\sqrt{(3 \cdot 19^2 + 26^2)}$ = 42 meV or FWHM = $\sqrt{(3 \cdot 26^2)}$ = 45 meV. In this case the measured resolution is about 40% worse than the total energy uncertainty due to the bandwidth of the short femtosecond laser pulses. Still the relative energy resolution of our electron imaging detection for electrons near 2 eV of $\Delta E_{FWHM}/E = 65/1870 = 3.5\%$ is very good and it shows that our lenses operate at good energy resolution and only slightly above the laser bandwidth limit.

In the lower part of panel C various photoelectron peaks, labeled (d)-(e), are observed resulting from the photoionization of NO. A progression of Franck-Condon off-diagonal Δv=1,2,3 peaks are observed when the centre wavelength of the laser pulses are carefully tuned to 399.8 nm and 266.3 nm. The probable cause for the strong $\Delta v \neq 0$ progression is the excitation of a superexcited state at these wavelengths.

D. Photoelectron-photoion energy correlation

In Fig. 8 we show the correlated photoelectron-photoion electron distribution of electrons and NO^+ ions from the multi-photon multi-channel photoexcitation in NO_2. The femtosecond laser pulses were time delayed by about 200 fs, with the 400 nm laser pulse before the 266 nm pulse. As can be seen in Fig. 8 many features are observed in the energy correlation plot, which are due to various multi-photon processes. For a detailed discussion of the molecular processes in NO_2 we refer to a recently published paper.[37]

Acknowledgments

This research has been financially supported by the council for Chemical Sciences of the Netherlands Organization for Scientific research (NWO–CW VICI program). WGR gratefully acknowledges the support of the European Union through a Marie Curie Outgoing International Fellowship under contract OIF 021907. The authors would like to thank dr. C.C. Hayden for many helpful discussions on coincidence imaging. WGR would like to thank dr. D. W. Chandler and dr. C. C. Hayden for the opportunity to visit and work at the Combustion Research Facility of Sandia National Laboratories Livermore. The authors would like to thank MSc. D. Irimia for extensive experiments on the MCP pickup signal. MHMJ would like to thank dr. A. Bergmann (Becker&Hickl) for the initial loan of the SPC-130 board for compatibility testing in our apparatus, dr. A. S. Tremsin for discussions on MCP electron cloud footprints, and mr. R. Cochran (Photonis) for discussions on MCP responses.

[1] D. W. Chandler and P. L. Houston, J. Chem. Phys. **87**, 1445 (1987).

[2] M. N. R. Ashfold, N. H. Nahler, A. J. Orr-Ewing, O. P. J. Vieuxmaire, R. L. Toomes, T. N. Kitsopoulos, I. A. Garcia, D. A. Chestakov, S.-M. Wu, and D. H. Parker, Phys. Chem. Chem. Phys **8**, 26 (2006).

[3] J.A. Davies, J.E. LeClaire, R.E. Continetti and C.C. Hayden, J. Chem. Phys. **111**, 1 (1999).

[4] R.E. Continetti, Ann. Rev. Phys. Chem. **52**, 165 (2001).

[5] A. M. Rijs, M. H. M. Janssen, E. T. H. Chrysostom, and C. C. Hayden, Phys. Rev. Lett. **92**, 123002 (2004).

[6] O. Gessner, A. M. D. Lee, J. P. Shaffer, S. V. Reisler, S. V. Levchenko, A. I. Krylov, J. G. Underwood, H. Shi, A. L. L. East, D. M. Wardlaw, et al., Science **311**, 219 (2006).

[7] M. Takahashi, J.P. Cave and J.H.D. Eland, Rev. Sci. Instrum. **71**, 1337 (2000).

[8] M. Lebech, J.C. Houver and D. Dowek, Rev. Sci. Instrum. **73**, 1866 (2002).

[9] R. E. Continetti and C. C. Hayden, Coincidence imaging techniques, in *Modern Trends in Reaction Dynamics*, Eds. X. Yang and K. Liu, World Scientific (Singapore), 2004, pp 475-528.

[10] K. Ueda, J. Electron Spectrosc. Relat. Phenom. **141**, 73 (2004).

[11] G. A. Garcia, L. Nahon, C. J. Harding, E. A. Mikajlo, and I. Powis, Rev. Sci. Instrum. **76**, 053302 (2005).

[12] K. Hosaka, J. Adachi, A. V. Golovin, M. Takahashi, N. Watanabe, and A. Yagashita, Jap. J. Applied Physics **45**, 1841 (2006).

[13] G. Prumper, H. Fukuzawa, T. Lischke, and K. Ueda, Rev. Sci. Instrum. **78**, 083104 (2007).

[14] D. Ceolin, G. Chaplier, M. Lemonnier, G. A. Garcia, C. Miron, L. Nahon, M. Simon, N. Leclercq, and P. Morin, Rev. Sci. Instrum. **76**, 043302 (2005).

[15] O. H. W. Siegmund, A. Tremsin, J. V. Vallerga, R. Abiad, and J. S. Hull, Nucl. Instr. Meth. Phys. Res. A **504**, 177 (2003).

[16] I. Ali, R. Dorner, O. Jagutzki, S. Nuttgens, V. Mergel, L. Spielberger, K. Khayyat, T. Vogt, H. Brauning, K. Ullmann, et al., Nucl. Instr. Meth. Phys. Res. B **149**, 490 (1999).

[17] A. Tremsin, G. Lebedev, O. Siegmund, J. Vallerga, J. Hull, J. McPhate, C. Jozwiak, Y. Chen, J. Guo, Z. Shen, et al., Nucl. Instr. Meth. Phys. Res. A **580**, 853 (2007).

[18] A. T. J. B. Eppink and D. H. Parker, Rev. Sci. Instrum. **68**, 3477 (1997).

[19] http://doc.cern.ch//archive/electronic/other/generic/public/cer-002723234.pdf.

[20] A. V. Akindinov and *et al.*, Nucl. Instr. Meth. Phys. Res. A **533**, 178 (2004).

[21] http://www.roentdek.com/.

[22] K. Inami, N. Kishimoto, Y. Enari, M. Nagamine, and T. Ohshima, Nucl. Instr. Meth. Phys. Res. A **560**, 303 (2006).

[23] A. Martindale, J. S. Lapington, and G. W. Fraser, Nucl. Instr. Meth. Phys. Res. A **573**, 111 (2007).

[24] http://www.becker-hickl.de/handbook.htm.

[25] R.S. Gao, P.S. Gibner, J.H. Newman, K.A. Smith and R.F. Stebbings, Rev. Sci. Instr. **55**, 1756 (1984).

[26] A. Tremsin, O. H. W. Siegmund, J. V. Vallerga, J. S. Hull, and R. Abiad, IEEE Trans. Nucl. Science **71**, 1707 (2003).

[27] In this paper we use, as is commonly done, a Gaussian distribution defined by $f(x) \propto exp(-x^2/2\sigma^2)$, from which the Full-Width-Half-Maximum can be obtained, FWHM $= 2.355\sigma$.

[28] W. C. Wiley and I. H. Mclaren, Rev. Sci. Instrum **16**, 1150 (1955).

[29] W. G. Roeterdink and M. H. M. Janssen, Phys. Chem. Chem. Phys. **4**, 601 (2002).

[30] W. G. Roeterdink and M. H. M. Janssen, J. Chem. Phys. **117**, 6500 (2002).

[31] W. G. Roeterdink, A. M. Rijs, and M. H. M. Janssen, J. Am. Chem. Soc. **128**, 576 (2006).

[32] A. Tremsin, O. Siegmund, J. Hull, J. Vallerga, J. McPhate, J. Soderstrom, J.-W. Chiou, J. Guo, and Z. Hussain, IEEE Trans. Nucl. Science **54**, 706 (2007).

[33] G. Lebedev, A. Tremsin, O. Siegmund, Y. Chen, Z. Shen, and Z. Hussain, Nucl. Instr. Meth. Phys. Res. A **582**, 168 (2007).

[34] T. Credo, H. Frisch, H. Sanders, R. Schroll, and F. Tang, Proceedings of the IEEE (Rome), Nuclear Science Symposium Conference Record **1** (2004).

[35] J.L. Wiza, Nucl. Instrum. Methods **162**, 587 (1979).

[36] G.W. Fraser, Nucl. Instr. Meth. Phys. Res. **A291**, 595 (1990).

[37] A. Vredenborg, W. G. Roeterdink, and M. H. M. Janssen, J. Chem. Phys. **128**, issue 7 June (2008).

FIGURE CAPTIONS

FIG.1 : (Color online) Schematic overview of the coincidence imaging machine for femtosecond time-resolved experiments in a molecular beam. The apparatus consists of three differentially pumped chambers, labeled (a) source chamber, (b) buffer chamber, (c) detection chamber. The total distance between the exit of the molecular beam nozzle and the laser interaction zone is 450 mm. Note that the dimensions in this overview are not to scale. On the ports labeled I, II and III the magnetically levitated turbo pumps are mounted with pumping speeds of 1250, 400 and 2100 l/s, respectively.

FIG.2 : Schematic overview of the charged particle lenses and the TOF-tube for ions and electrons. The plates are 2 mm thick. All lenses are open and no grids are used anywhere in the apparatus. All indicated distances are in mm. The subscript e labels the electron lenses and detector, the subscript i labels the ion lenses and detector. The centre of the ion detector is displaced by about 7-8 mm relative to the centre of the electron detector to compensate for the forward center-of-mass velocity of the molecular beam when detecting ions.

FIG.3 : Time-Of-Flight spectrum of Xenon isotopes recorded in coincidence with electrons, i.e. with switching the electric fields on the lenses. The arrival time is measured from the average of the time-sum from the delay line signals as obtained with the TDC. The TOF peaks have a typical FWHM Δt = 2 ns, the total TOF time is about t = 8.3 μs. This means we have a mass resolution, $\Delta m_{FWHM}/m = 1/4150$ for masses near m = 130 amu.

FIG.4 : (Color online) The focus of the Xe^+ parent ion spot as measured in coincidence on the ion detector with our typical voltages used on the lenses for coincidence imaging. The vertical axis gives the velocity map focus perpendicular to the direction of the molecular beam. We obtain a smallest focussed spot of about σ = 115 μm (FWHM = 270 μm) from the initially extended source region, defined by the crossing of the molecular beam with the laser, which is estimated to be about 1 mm along the laser propagation direction. The spot size of σ = 285 μm (FWHM = 670 μm) in the horizontal direction reflects the longitudinal

velocity spread in the molecular beam (see text). The total region of the ion image shown is a 5 by 5 = 25 mm^2 cut, the total ion image has a diameter of 40 mm, i.e. an area of 1257 mm^2.

FIG.5 : (Color online) Time-Of-Flight distribution of electron measured in coincidence with Xe ions under our typical voltages used for electron imaging (see text). The distribution in panel a) is measured by taking the pickup signal from the back MCP plate which is pre-amplified and processed by the TAC (B&H SPC-130). The distribution in panel b) is obtained from the average of the time-sum in one direction as measured on the delay line signals by the 8-channel TDC (Roentdek TDC8HP). For the channel width of the TAC we used a least-significant-bit of 1 channel bin = 813.8 fs, for the TDC we used 1 channel bin = 25.0 ps, both values are as specified by the manufacturers. The polarization of the 400 nm femtosecond laser was oriented along the TOF axis, resulting in a forward ejected electron and a backward ejected electron. It is clear that the TAC measurement gives the highest resolution electron TOF distribution. The colored solid lines (red for forward and green for backward electron distribution) are Gaussian curves with a fitted resolution[27] of σ = 20 ps and 18 ps for the forward and backward electron peak, respectively. SIMION simulations with our lenses and voltages used give a very similar forward-backward time of 540 ps as is measured experimentally. It means that the electron which is ejected with 0.285 eV is formed in the acceleration region between R_e and E_e at a field strength of about 6.7 Volt/mm.

FIG.6 : (Color online) Best Time-Of-Flight distribution of electrons in coincidence with Xe ions as measured with the TAC but now at higher acceleration voltages on the lenses (acceleration field between R_e and E_e is about 19 Volt/mm). This graph shows our currently best arrival time distribution for electrons. The measured resolution of σ = 16 ps represents the temporal uncertainty of a single electron hit on the electron detector. The uncertainty is mostly caused by the transit-time-spread in our 5μm MCPs of a single electron hit on the electron detector (see text). At these acceleration fields the forward backward time difference is reduced to about 188 ps.

FIG.7 : (Color online) A) Time sliced electron image in coincidence with Xe ions. B) A time sliced electron image in coincidence with NO ions. C) The corresponding energy distributions derived from A) and B). The FWHM width of the electron peak

near 1.87 eV, labeled (c), represents an energy resolution of $\Delta E_{FWHM}/E = 65/1870 = 3.5\%$.

FIG.8 : (Color online) Energy correlation plot of electrons and coincident NO^+ ions produced in a two-color femtosecond pump-probe experiment on NO_2. The time delay between the 400 nm pump and the 266 nm probe is 200 fs. The red line represents the maximum available energy for a process involving 3 photons of 400 nm and 1 photon of 266 nm, a (3+1') process, leading to NO^+(v=0) + O(^{3}P); the green line represents the maximum available energy for a process involving 2 photons of 400 nm and 2 photons of 266 nm, a (2+2') process, leading to NO^+(v=1) + O(^{3}P). A detailed discussion of the various multi-photon multi-channel dissociation and pathways leading to the formation of the specific photoelectron-photoion regions is presented elsewhere.[37]

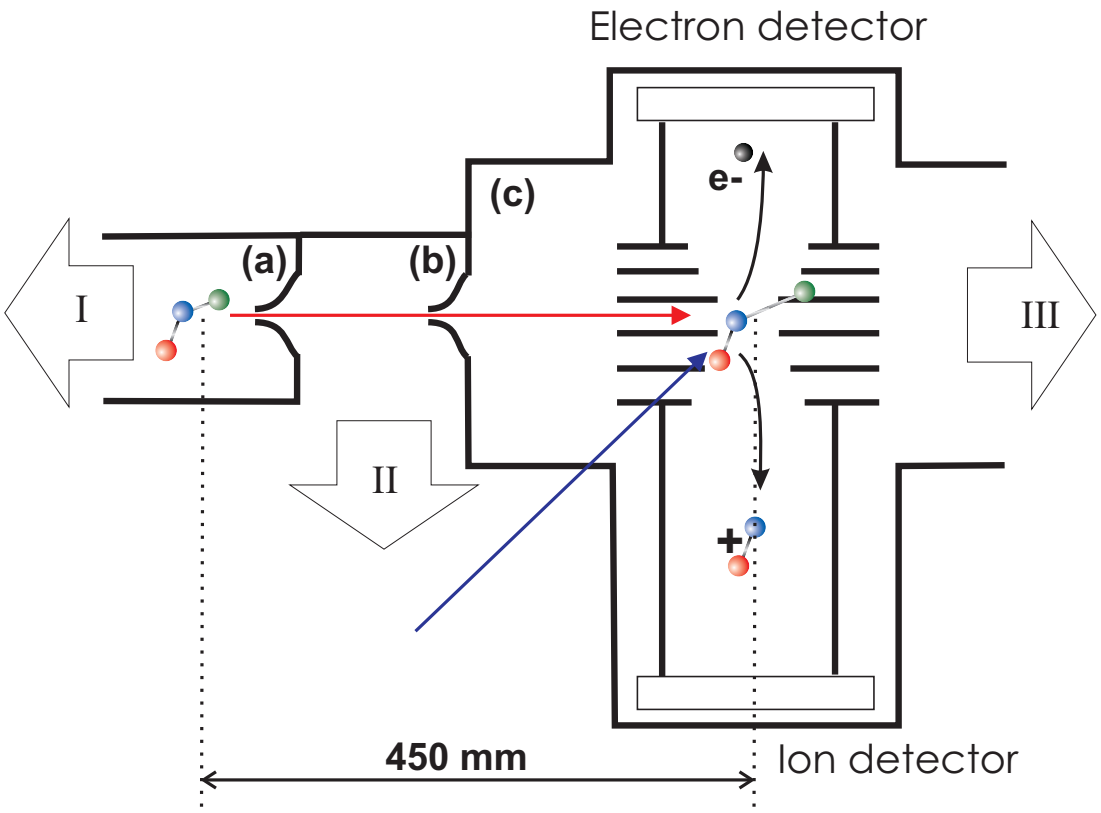

FIG. 1: Vredenborg *et al.*, A photoelectron–photoion coincidence imaging apparatus...

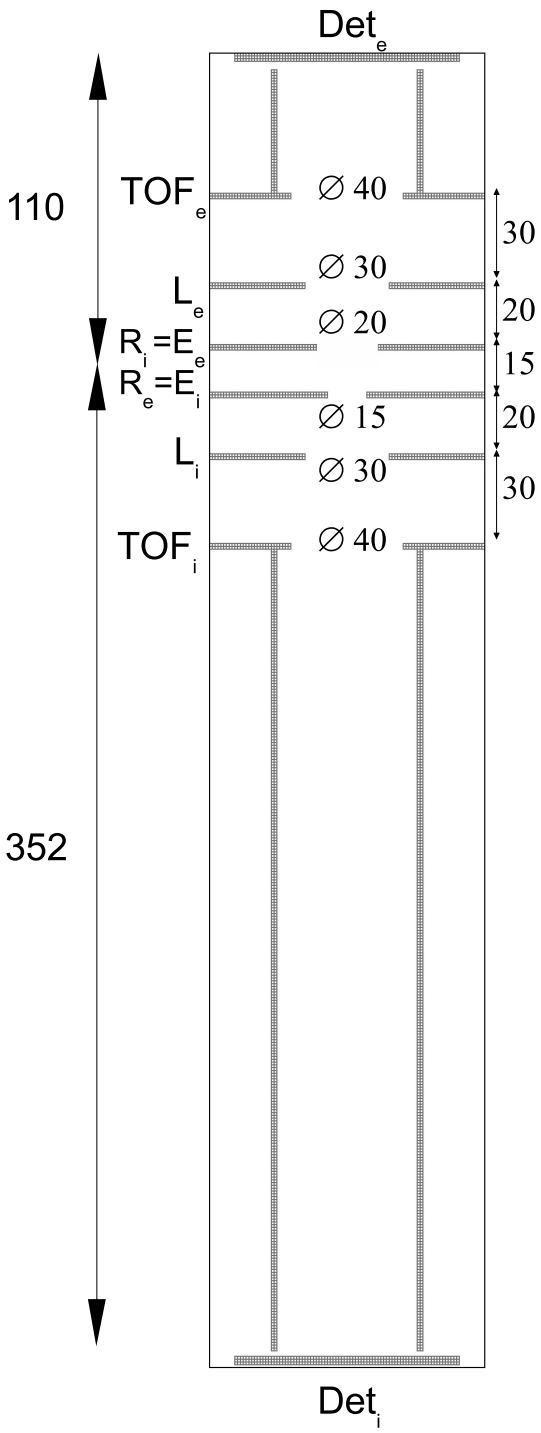

FIG. 2: Vredenborg *et al.*, A photoelectron–photoion coincidence imaging apparatus...

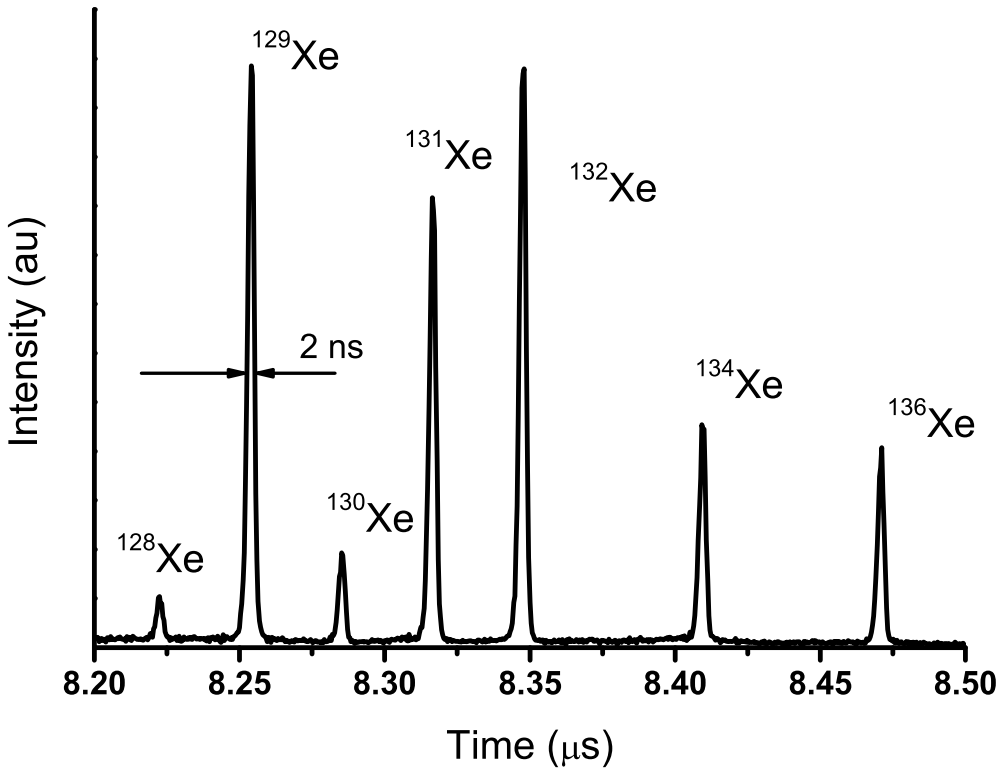

FIG. 3: Vredenborg *et al.*, A photoelectron–photoion coincidence imaging apparatus...

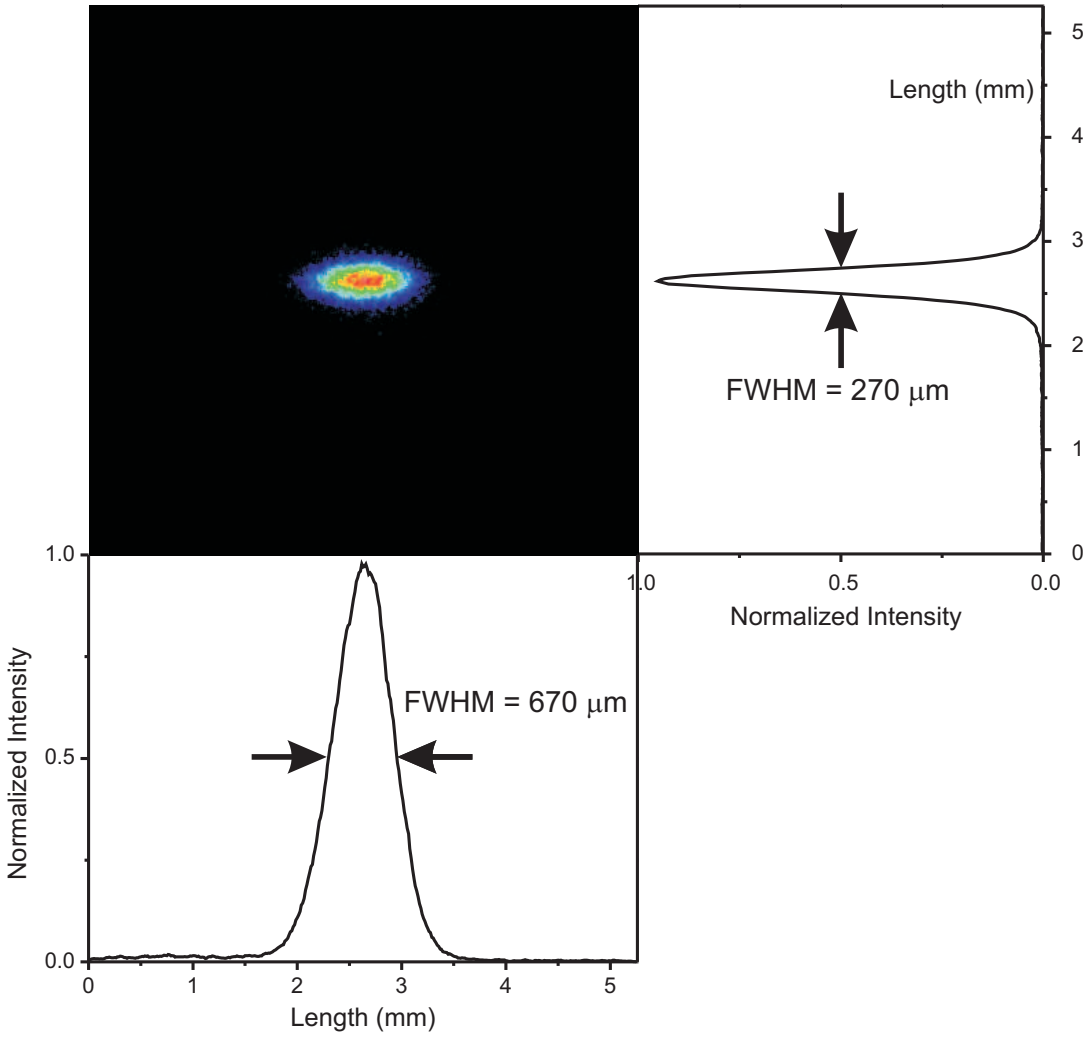

FIG. 4: Vredenborg *et al.*, A photoelectron–photoion coincidence imaging apparatus...

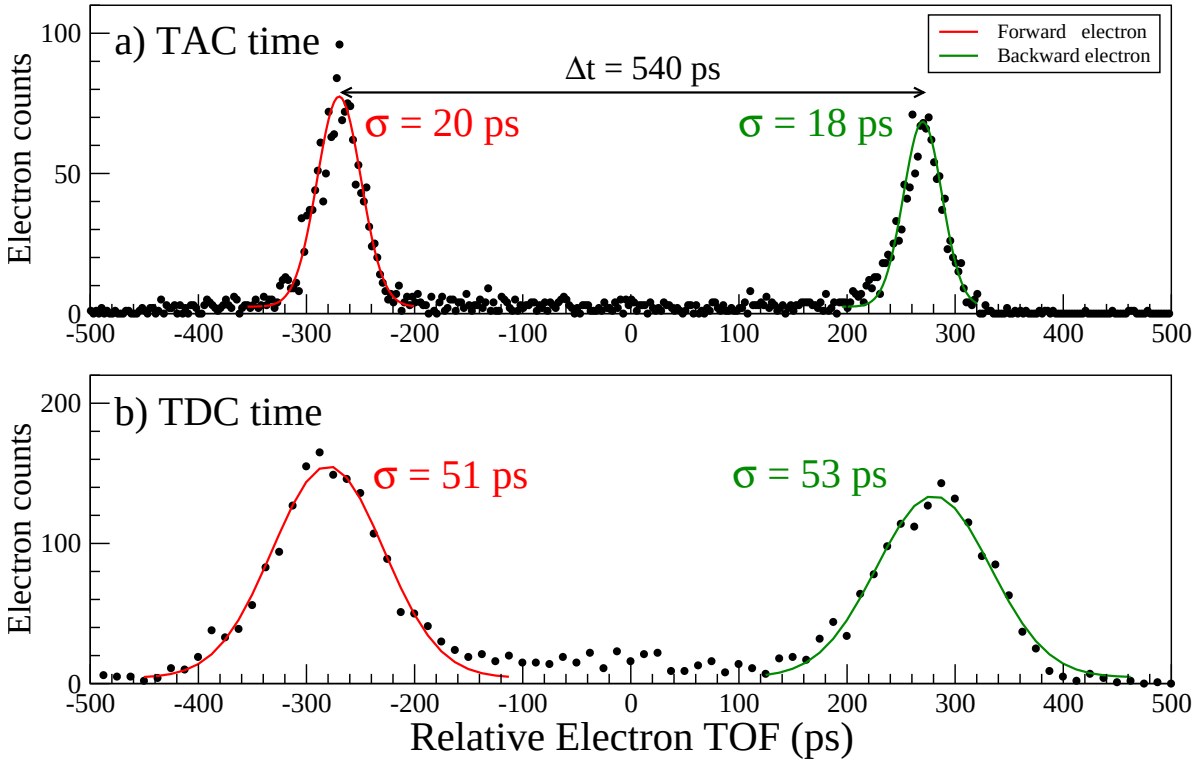

FIG. 5: Vredenborg *et al.*, A photoelectron–photoion coincidence imaging apparatus...

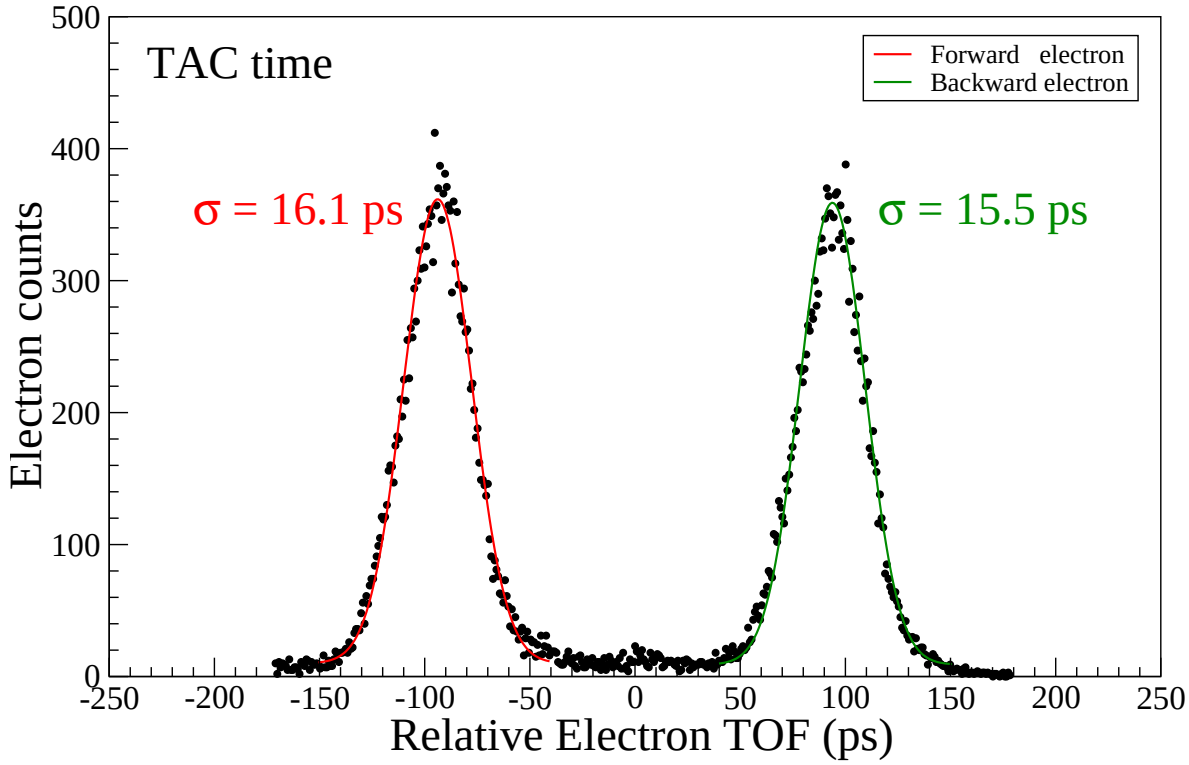

FIG. 6: Vredenborg *et al.*, A photoelectron–photoion coincidence imaging apparatus...

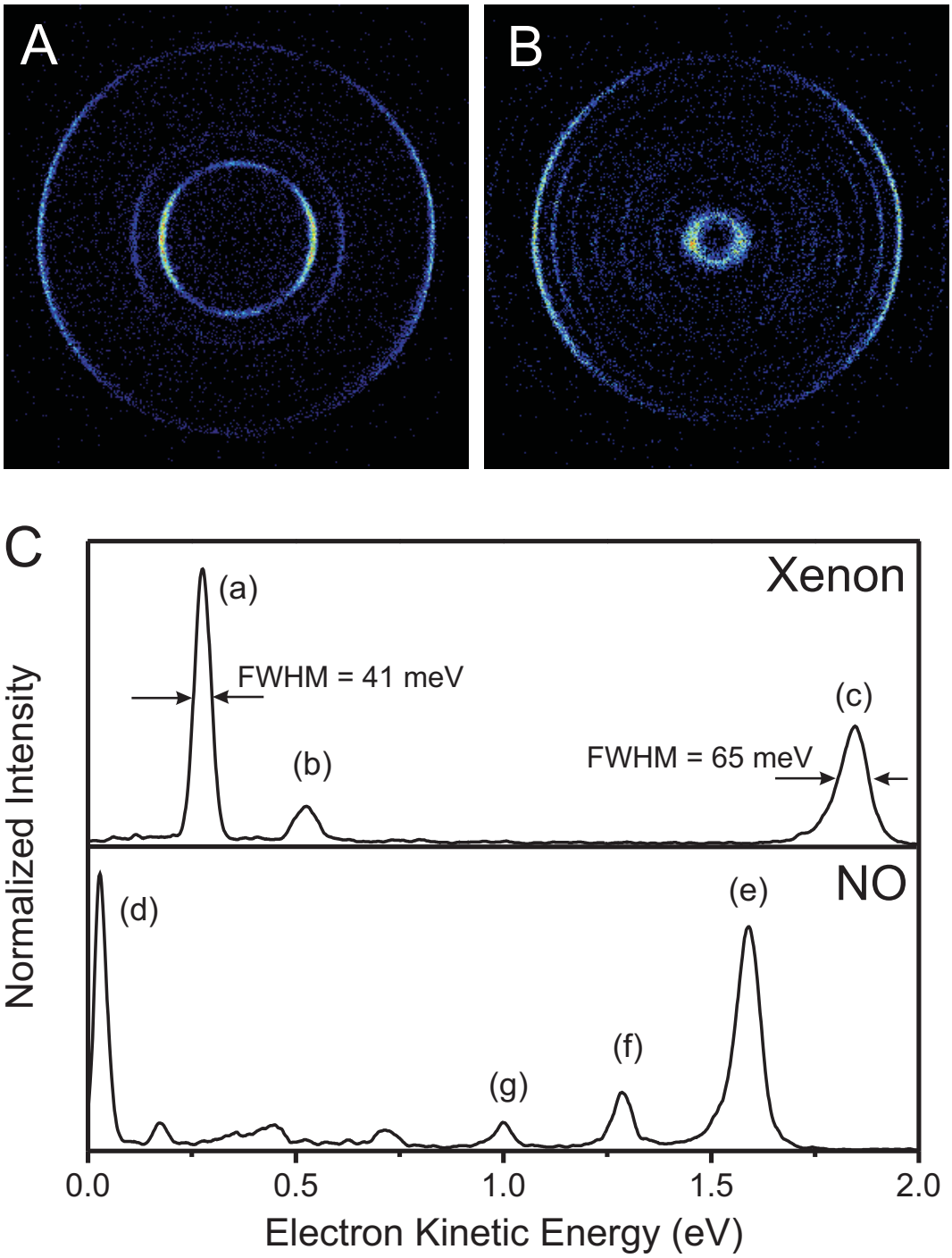

FIG. 7: Vredenborg *et al.*, A photoelectron–photoion coincidence imaging apparatus...

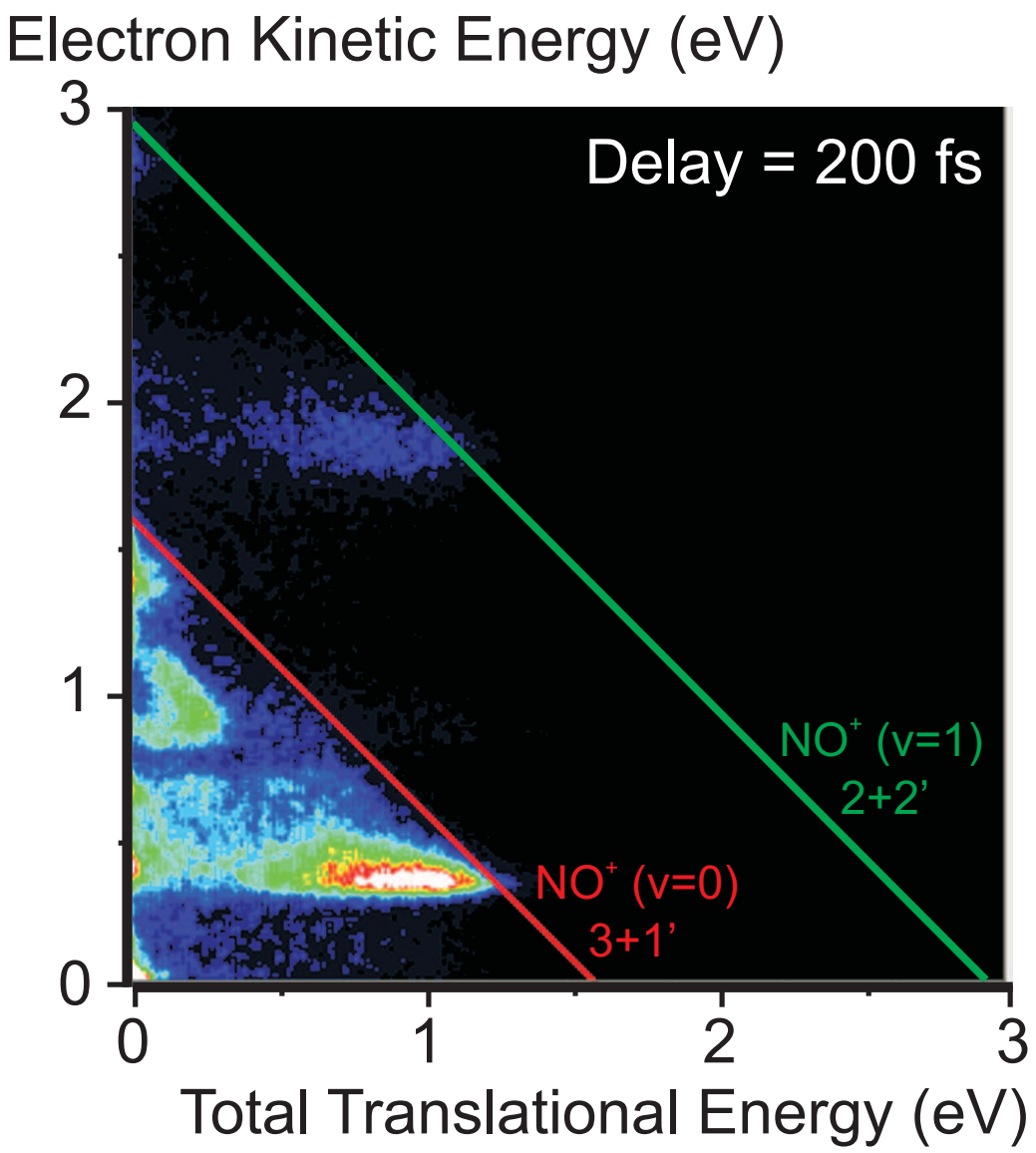

FIG. 8: Vredenborg *et al.*, A photoelectron–photoion coincidence imaging apparatus...